applied optics

Optical design of a cooled mid-wave infrared off-axis three-mirror system with a low F-number and wide field of view

Yunqiang Xie,[1,2,3] Chunyu Liu,[1,3,*] Shuai Liu,[1,3] Minglin Xu,[1,3] Xinghao Fan,[1,2,3] and Qilong Rao[4]

[1]Changchun Institute of Optics, Fine Mechanics and Physics, Chinese Academy of Sciences, Changchun 130033, China
[2]University of Chinese Academy of Sciences, Beijing 10049, China
[3]National & Local United Engineering Research Center of Small Satellite Technology, Changchun 130033, China
[4]Shanghai Institute of Satellite Engineering, Shanghai, 201109, China
*Corresponding author: mmliucy@163.com

Received 29 November 2021; revised 24 December 2021; accepted 3 January 2022; posted 6 January 2022; published 24 February 2022

Infrared imaging systems with a wide detection scale, excellent precision, and high resolution are playing an increasingly important role in many fields. Compared with uncooled infrared detectors, the cooled infrared detectors have the advantages of high precision, long detection distance, and a high signal-to-noise ratio due to the low working temperature. In this paper, a cooled off-axis three-mirror mid-wave infrared (MWIR) optical system with a wide field of view (FOV), long focal length, and large relative aperture is designed. We first establish the initial coaxial three-mirror system based on the third-order Seidel aberration theory and then make the aperture stop offset to eliminate central obscuration. During the process of optimization, the FOV of the system is expanded stepwise, and it is not biased to avoid the extra aberration. In order to increase the optimizing degrees of freedom to improve the aberration elimination ability of the system, we apply the *XY* polynomial surface on the tertiary mirror (TM). After optimization, we finally obtain a cooled off-axis three-mirror MWIR optical system with a FOV of 5.3° × 4.4°, a focal length of 500 mm, and a relative aperture of 1/2. The image quality of our system is excellent, and the aperture stop is between the focal plane and the TM, and coaxial with the focal plane, meeting the conditions of matching with the cold stop of the infrared detector. The tolerance analysis is also carried out, and the result shows that the system meets the requirements of practical fabrication and alignment. © 2022 Optica Publishing Group

https://doi.org/10.1364/AO.449841

1. INTRODUCTION

Objects with temperatures above absolute zero produce infrared radiation all the time. Infrared detection technology has been widely used in many fields such as fire monitoring, medical diagnosis, national defense, and geological prospecting [1–5]. Compared with visible light imaging technology, infrared detection can be applied in a low-illumination environment and under harsh conditions, including mist and haze for its excellent transmittance in such conditions. Besides, infrared detection does not need to emit electromagnetic waves and thus has excellent concealment compared with ratio detection.

According to the working temperature of the pixel array, infrared image detectors can be divided into cooled and uncooled types. Cooled infrared image detectors usually operate in a low temperature of less than 77 K, while the working temperature of the uncooled detectors is usually room temperature and will rise with the increase of working time and thus generate extra noise [6,7]. Compared with the infrared imaging systems with uncooled image detectors, those with cooled image detectors have more excellent detection accuracy and thus have been widely used in high-precision aerial and space remote sensing [8,9]. Besides, the cold stop of the cooled detector can match with the exit pupil or aperture stop of an optical system to efficiently suppress stray radiation.

Optical systems mainly can be divided into two categories: refractive systems and reflective systems. The refractive systems possess the characteristics of easy design and alignment, low cost, and no central obscuration, and thus have been used in many fields [10–12]. However, for the infrared optical systems, the applicable materials are very rare, and most of them have low transmittance and a high price. When used in systems with a long focal length and low F-number, which contain the optical lenses with large aperture, the structural and thermal stability of the system will decrease sharply, and the secondary spectrum is difficult to eliminate [13,14]. Compared with refractive systems, reflective optical systems have advantages in terms of better thermal performance, a wider working spectrum range, and a lower ratio of the system length to the focal length [15–17]. Off-axis reflective optical systems evolve from

coaxial reflective systems by making the aperture stop offset or FOV biased to avoid the central obscuration and have received increased attention of researchers because of its incomparable advantages: more effective aperture, high degrees of design freedom, and better spot diagram energy concentration [18–20]. These features enable off-axis reflective optical systems to have a wide FOV, long focal length, large relative aperture, and more compact volume than the refractive systems with the same specifications.

Based on the analysis above, a cooled off-axis three-mirror optical system is an ideal scheme to realize infrared detection with a wide detection scale, excellent precision, and high resolution. At present, the off-axis optical systems are usually used in an uncooled infrared system and rarely in a cooled system. Lacy G. Cook presented a cooled off-axis three-mirror optical system, but the focal plane and the aperture stop of the system are not coaxial, and the cooled infrared detector has to apply off-axis Dewar which leads to high cost [21]. Lacy G. Cook designed a cooled off-axis four-mirror optical system later and made the focal plane coaxial with the aperture stop, but the design method is not presented [22]. Yu has designed a cooled off-axis three-mirror optical system with a linear FOV of 7° × 0.2° and a relative aperture of 1/4 [23]. The linear FOV means that the system can only work in scanning mode, and the low relative aperture will limit the signal-to-noise ratio and detection distance. Jiang has designed a cooled off-axis three-mirror optical system with a rectangular FOV of 3.662° × 2.931°, a relative aperture of 1/2, and a focal length of 450 mm [24]. Chao has presented a cooled off-axis three-mirror optical system with a rectangular a FOV of 5° × 3°, a relative aperture of 1/2.5, and a focal length of 300 mm [25]. These two systems have a certain degree of upgrade compared to the previous systems.

In this paper, a low F-number cooled off-axis three-mirror mid-wave infrared (MWIR) optical system with a wide rectangular FOV and a long focal length is presented; the design method is also described in detail. The F-number of this system is 2, the spectral range is 3.7 μm–4.8 μm, the FOV is 5.3° × 4.4°, and the focal length is 500 mm. Compared with long-wave infrared (LWIR), MWIR has higher transmittance in humid and hot atmosphere and thus is more suitable for detecting desert and sea areas. In addition, MWIR can achieve higher resolution than LWIR due to its shorter wavelength. We have determined the optical specifications of the system based on the technical index and then established the initial configuration based on the third-order Seidel aberration theory. For the purpose of suppressing stray radiation, the exit pupil or aperture stop should be set between the tertiary mirror (TM) and the focal plane to match with the cold stop of the cooled detector. Since the exit pupil is the image formed by the aperture stop through the optical elements behind it and is usually not perfect [26], the shape of the exit pupil is irregular, and thus will reduce the matching efficiency. Therefore, we set the aperture stop between the TM and the focal plane. After the initial configuration is obtained, we make the aperture stop offset to eliminate central obscuration and then expand the FOV step by step. During the process of optimization, the operands and constraints provided by optical design software are used to constrain the optical and geometric features of the system and meanwhile correct aberrations. The XY polynomial surface is used to increase the optimizing degrees of freedom so as to improve the aberration correction ability of the system. After iterative optimization in optical design software, we get the final optical system with excellent image quality. The tolerance analysis result shows that our system has good instrumentation feasibility.

2. OPTICAL SPECIFICATIONS AND SELECTION OF OPTICAL SCHEME

A. Optical Specifications

The schematic of the cooled infrared detector used in this paper is shown in Fig. 1, where the units of the data are all millimeters. The spectral range of the detector is 3.7–4.8 μm. The optical components of the detector mainly include the window glass, cold stop, and pixel array. The number of active pixels is 3000 × 2500, and each pixel size is 15 μm × 15 μm.

In order to achieve a high resolution, the focal length of the system f' is determined as 500 mm. At the same time, to ensure that the optical system matches the detector, the aperture stop is placed between the TM and the focal plane, and its diameter and position should be consistent with those of the detector's cold stop. Therefore, the diameter of the entrance pupil of the optical system D_E is given by

$$D_E = \frac{D_C \cdot f'}{H}, \tag{1}$$

where D_C is the diameter of the cold stop and aperture stop, H is the distance from the cold stop to the focal plane, i.e., the pixel array and their values are 50 and 100 mm, respectively, according to Fig. 1. It can be calculated that the diameter of the entrance pupil is 250 mm, and thus the F-number of the optical system is 2. The tangential and sagittal dimensions of the detector's pixel array are given by $L_t = 3000 \times 15\ \mu\text{m} = 45$ mm and $L_s = 2500 \times 15\ \mu\text{m} = 37.5$ mm; thus, the tangential FOV ω_t and sagittal FOV ω_s can be obtained as follows:

$$2\omega_t = 2\arctan\left(\frac{L_t}{2f'}\right) = 5.15°, \quad 2\omega_s = 2\arctan\left(\frac{L_s}{2f'}\right) = 4.3°. \tag{2}$$

We choose $2\omega_t$ and $2\omega_s$ as 5.3° and 4.4°, respectively, to have abundant detecting allowance, so the FOV of our system is 5.3° × 4.4°. In order to ensure the high-resolution imaging of the system, the modulation transfer function (MTF) of the system should be greater than 0.12 at the Nyquist frequency which is given as 33.3 lp/mm by

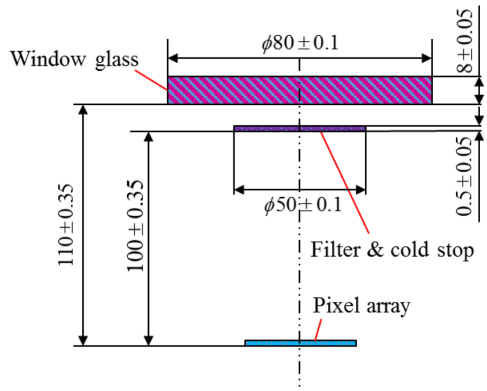

Fig. 1. Schematic of the cooled infrared detector.

Table 1. Optical Specifications of the Imaging System

Parameters	Specifications
Wavelength range/μm	3.7 to 4.8
Focal length/mm	500
F/#	2
FOV/°	5.3 × 4.4
Pixel size/μm	15
MTF	≥ 0.4 at 34 lp/mm

$$N = \frac{1000}{2 \cdot \alpha}, \tag{3}$$

where N is the Nyquist frequency, and α is the size of one single pixel. The MTF of the system is determined by [27]

$$\mathrm{MTF} = \mathrm{MTF}_{\mathrm{design}} \cdot \mathrm{MTF}_{\mathrm{man}} \cdot \mathrm{MTF}_{\mathrm{detector}}, \tag{4}$$

where $\mathrm{MTF}_{\mathrm{design}}$ is the design value of the MTF of the optical system, $\mathrm{MTF}_{\mathrm{man}}$ is the MTF of the optical system manufacturing which is usually 0.8 based on engineering experience [28], $\mathrm{MTF}_{\mathrm{detector}}$ is the MTF of the detector and the value is 0.5. The $\mathrm{MTF}_{\mathrm{design}}$ should be better than 0.3 at the Nyquist frequency through calculation. We choose $\mathrm{MTF}_{\mathrm{design}}$ as 0.4 at 34 lp/mm in order to have abundant allowance. The technical specifications of the optical system are listed in Table 1.

B. Selection of Optical Scheme

Off-axis three-mirror optical systems can be classified into relayed systems and non-relayed systems based on the presence or absence of the intermediate image plane [29], as shown in Fig. 2. In a relayed off-axis three-mirror optical system, the aperture stop is usually set in front of the primary mirror (PM) or between the TM and focal plane [30]. This system can easily achieve large relative aperture. In addition, since there is an intermediate image plane between the secondary mirror (SM) and the TM, a field stop can be placed in this position to suppress stray light. However, it is difficult for the system to achieve a wide FOV because the system is asymmetric and the size of the TM will increase sharply with the increase of the FOV. In a non-relayed system, the aperture stop is usually set at the SM, which means that the PM and the TM are symmetrical relative to the SM and thus can obtain a wide FOV [31,32]. However, for our system, in order to realize stop matching, the aperture stop must be placed between the TM and focal plane, which will make the aperture of the PM increase sharply in a non-relayed system. Besides, constrained by the size of the infrared detector's pixel array, the FOV of our system can be realized in a relayed system, and the diameter of the TM can be controlled within a reasonable range. Therefore, we choose the relayed off-axis three-mirror optical system as our design scheme.

3. ESTABLISHING INITIAL STRUCTURE BASED ON THIRD-ORDER SEIDEL ABERRATION THEORY

A proper starting point is critical to a successful optical design. We begin our optical system design by establishing a coaxial three-mirror system. In order to obtain an ideal initial structure, the relationship between aberrations and structure parameters of the coaxial three-mirror system should be built first. The ray tracing diagrams of the chief ray and marginal ray in the coaxial three-mirror system are shown in Fig. 3. u_i and $u_i'(i = 1, 2, 3)$ represent the incident angle and emergence angle, respectively, of the marginal ray on the PM, SM, and TM; $\bar{u}_i$ and $\bar{u}_i'$ represent the incident angle and emergence angle, respectively, of the chief ray.

The three mirrors are all designed as spherical surfaces in the initial structure. The marginal ray originates from the object point on the optical axis at infinity; thus, $u_1 = 0$. d_1 and d_2 are the distance between the PM and SM and the distance between the SM and TM, respectively. y_i and $\bar{y}_i$ represent the height of the marginal ray and chief ray, respectively, on the PM, SM, and TM, respectively. The curvature radii of the PM, SM, and TM are denoted by r_i. By tracing the paraxial rays, the relationship between the ray height, distance, and incident or emergence angle of different mirrors can be expressed as

$$\begin{cases} n_i' u_i' = n_i u_i - y_i \phi_i \\ n_i' \bar{u}_i' = n_i \bar{u}_i - \bar{y}_i \phi_i \\ y_{i+1} = y_i + u_i' d_i' \\ \bar{y}_{i+1} = \bar{y}_i + \bar{u}_i' d_i' \\ u_i' = u_{i+1} \\ \bar{u}_i' = \bar{u}_{i+1} \\ d_i' = d_{i+1} \end{cases}, \tag{5}$$

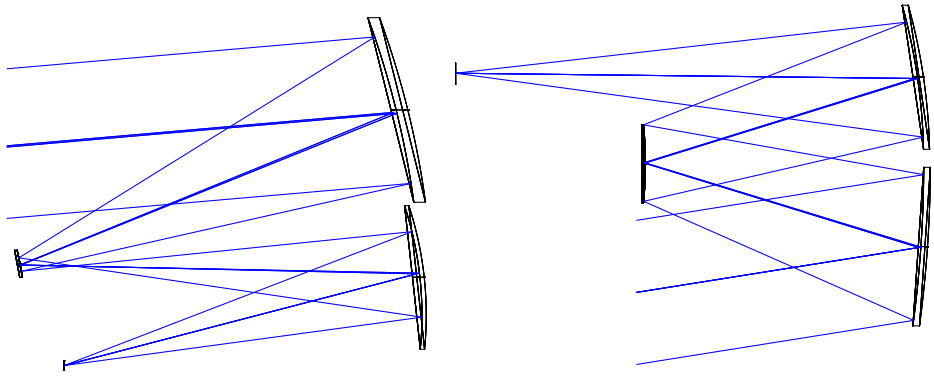

(a) (b)

Fig. 2. Two types of widely used off-axis three-mirror optical systems: (a) relayed off-axis three-mirror optical system and (b) non-relayed off-axis three-mirror system.

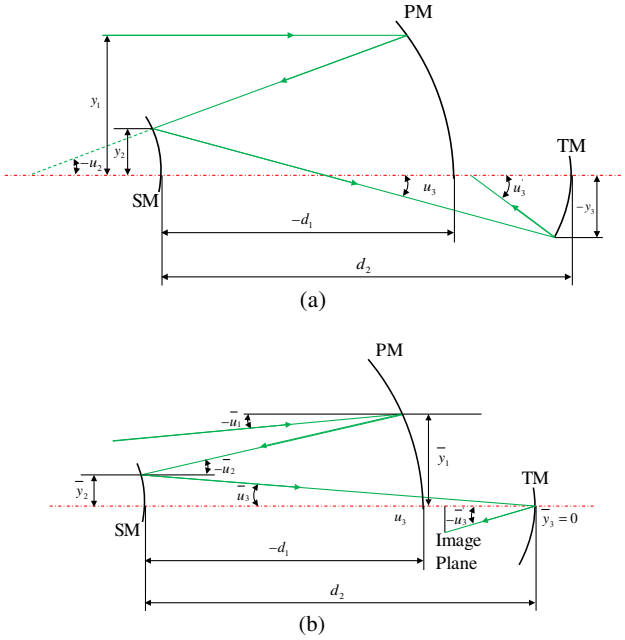

Fig. 3. Ray tracing of the initial coaxial three-mirror structure: (a) tracing of the marginal ray and (b) tracing of the chief ray.

where A is the Snell invariant of the marginal ray, B is the Snell invariant of the chief ray, L is the Lagrange invariant of the system, and C is the curvature of a mirror. The variables in Eq. (2) can be calculated by

$$\begin{cases} A = n(u + yC) \\ B = n\,(\overline{u} + \overline{y}C) \\ \Delta\left(\frac{u}{n}\right) = \frac{u'}{n'} - \frac{u}{n} \\ \Delta\left(\frac{1}{n}\right) = \frac{1}{n'} - \frac{1}{n} \\ L = n\overline{u}y - nu\overline{y} \end{cases}. \tag{8}$$

Among the five monochromatic aberrations, spherical aberration, coma, astigmatism, and Petzval field curvature will reduce the image quality, and our main purpose is to eliminate them. For distortion, it is a fixed value and only causes the deformation of the image without affecting the clarity of the image. The distortion can be measured accurately after system alignment. Based on the measurement result, the distortion can be eliminated by a specific image processing algorithm and thus is not considered in the stage of initial structure design. According to Eqs. (5)–(8), the relationship between Seidel aberration coefficients and parameters of the optical system can be expressed as

$$\begin{cases} S_{\mathrm{I}} = \frac{2y_1^4}{r_1^3}\Big[-1 + \frac{1}{r_1r_2^3}(r_1 - 2d_1)^2(2r_2 - r_1 + 2d_1)^2 - \frac{1}{r_1r_2^4r_3^3}(r_1r_2 - 2r_1d_2 - 2r_2d_1 + 2r_2d_2 + 4d_1d_2)^2 \\ \quad (r_1r_2 - 2r_1r_3 + 2r_2r_3 - 2r_1d_2 - 2r_2d_1 + 2r_2d_2 + 4r_3d_1 + 4d_1d_2)\Big] \\ S_{\mathrm{II}} = \frac{2y_1^3\overline{u_1}}{r_1^3}\Big[-\left(r_1 + \frac{\overline{y_1}}{\overline{u_1}}\right) + \frac{1}{\overline{u_1}r_1r_2^3}(r_1 - 2d_1)^2(2r_2 - r_1 + 2d_1)\,(\overline{u_1}r_1r_2 - r_1\overline{y_1} + \overline{u_1}r_1d_1 + 2r_2\overline{y_1} + 2d_1\overline{y_1}) \\ \quad -\frac{1}{\overline{u_1}r_1r_2^4r_3^3}(r_1r_2 - 2r_1d_2 - 2r_2d_1 + 2r_2d_2 + 4d_1d_2)^2\,(\overline{u_1}r_1r_2r_3 + r_1r_2\overline{y_1} - \overline{u_1}r_1r_2d_1 - 2r_1r_3\overline{y_1} + \overline{u_1}r_1r_2d_2 \\ \quad + 2\overline{u_1}r_1r_3d_1 + 2\overline{y_1}r_2r_3 - 2\overline{y_1}r_1d_2 - 2\overline{y_1}r_2d_1 + 2\overline{u_1}r_1d_1d_2 + 2\overline{y_1}r_2d_2 + 4\overline{y_1}r_3d_1 + 4\overline{y_1}d_1d_2) \\ \quad (r_1r_2 - 2r_1r_3 + 2r_2r_3 - 2r_1d_2 - 2r_2d_1 + 2r_2d_2 + 4r_3d_1 + 4d_1d_2)\Big] \\ S_{\mathrm{III}} = \frac{2y_1^3\overline{u_1}^2}{r_1^3}\Big[-\frac{1}{\overline{u_1}^2}(\overline{u_1}r_1 + \overline{y_1})^2 + \frac{1}{\overline{u_1}^2r_1r_2^3}(r_1 - 2d_1)^2(\overline{u_1}r_1r_2 - r_1\overline{y_1} + \overline{u_1}r_1d_1 + 2r_2\overline{y_1} + 2d_1\overline{y_1})^2 \\ \quad -\frac{1}{\overline{u_1}^2r_1r_2^4r_3^3}(r_1r_2 - 2r_1d_2 - 2r_2d_1 + 2r_2d_2 + 4d_1d_2)^2\,(\overline{u_1}r_1r_2r_3 + r_1r_2\overline{y_1} - \overline{u_1}r_1r_2d_1 - 2r_1r_3\overline{y_1} + \overline{u_1}r_1r_2d_2 \\ \quad +2\overline{u_1}r_1r_3d_1 + 2\overline{y_1}r_2r_3 - 2\overline{y_1}r_1d_2 - 2\overline{y_1}r_2d_1 + 2\overline{u_1}r_1d_1d_2 + 2\overline{y_1}r_2d_2 + 4\overline{y_1}r_3d_1 + 4\overline{y_1}d_1d_2)^2\Big] \\ S_{\mathrm{IV}} = \frac{2y_1^2\overline{u_1}^2}{r_1r_2r_3}\,(r_1r_2 - 2r_1r_3 + 2r_2r_3) \end{cases}. \tag{9}$$

where n_i and n_i' are the transmission media refractive indices of each mirror in object space and image space, respectively. In a three-mirror system, $n_1 = n_2' = n_3 = 1$, and $n_1' = n_2 = n_3' = -1$. ϕ_i is the optical power of each mirror, which can be expressed by the curvature of the mirror C_i as

$$\phi_i = \left(n_i' - n_i\right) \cdot C_i = \frac{n_i' - n_i}{r_i}. \tag{6}$$

According to the Seidel aberration theory, the third-order aberration coefficients, namely, Seidel spherical coefficient S_{I}, Seidel coma coefficient S_{II}, Seidel astigmatism coefficient S_{III}, Seidel Petzval field curvature coefficient S_{IV}, and Seidel distortion coefficient S_{V} can be expressed by the following:

$$\begin{cases} S_{\mathrm{I}} = -\sum A^2 \cdot y \cdot \Delta\left(\frac{u}{n}\right) \\ S_{\mathrm{II}} = -\sum A \cdot B \cdot y \cdot \Delta\left(\frac{u}{n}\right) \\ S_{\mathrm{III}} = -\sum B^2 \cdot y \cdot \Delta\left(\frac{u}{n}\right) \\ S_{\mathrm{IV}} = -L^2 \sum C \cdot \Delta\left(\frac{1}{n}\right) \\ S_{\mathrm{V}} = -\sum \frac{B}{A}\left[C \cdot L^2\Delta\left(\frac{1}{n}\right) - B^2 \cdot y \cdot \Delta\left(\frac{u}{n}\right)\right] \end{cases}. \tag{7}$$

In order to obtain an initial structure with minimal aberration, we minimize the Seidel aberration coefficients in Eq. (9) under the given reasonable values of y_1, $\bar{y}_1$, and $\bar{u}_1$ to get parameters of the coaxial three-mirror system. In addition, we set the TM as the aperture stop to simplify the process of placing the aperture stop between the TM and the image plane in the later design. Thus, the system should satisfy $\bar{y}_3 = 0$, which can be expressed as

$$\overline{y_3} = \overline{y_1} + \overline{u_1}(d_2 - d_1) + \frac{1}{r_1r_2}\left(4\overline{y}_1d_1d_2 - 2\overline{y}_1d_1r_2 + 2\overline{y}_1d_2r_2 - 2\overline{y}_1d_2r_1 + 2d_1d_2r_1\overline{u}_1\right) = 0. \tag{10}$$

For the focal length of the system, we add the following equation to constrain:

$$f' = \frac{y_1}{u_3'} = -500. \tag{11}$$

According to Eq. (3), it can be rewritten as

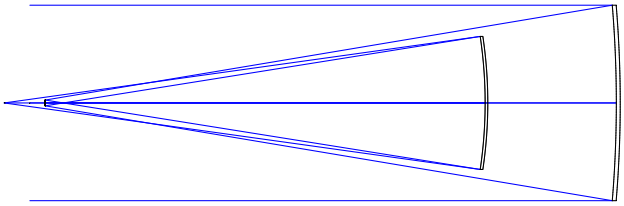

Fig. 4. Optical layout of the initial coaxial three-mirror system.

Table 2. Initial Structure Parameters

Surface	Radius (mm)	Distance (mm)	Conic
PM	−835.429	−405.067	−0.739
SM	−548.646	312.004	−0.054
TM	−318.524	−341.109	−0.070

$$\frac{1000}{r_1 r_2 r_3}\left(r_2 r_3 - r_1 r_3 + 2r_3 d_1 + r_1 r_2 + 2r_2 d_1 + 2r_2 d_2 - 2r_1 d_2 + 4d_1 d_2\right) = 1. \tag{12}$$

In the system, there are five variables, r_1, r_2, r_3, d_1, and d_2. Hence, constraints on the position of the aperture stop and focal length are necessary, and we can only set three Seidel aberration coefficients to zero to get parameters of the initial structure. Given that spherical aberration is on-axis aberration and is relatively easily corrected, we set S_{II}, S_{III}, and S_{IV} in Eq. (9) to zero and combine them with Eqs. (10) and (12) to obtain the initial optical structure.

In our system, the initial values of y_1, $\bar{y}_1$, and $\bar{u}_1$ are set to 150 and 25 mm, and 0.5°, respectively, to solve the configuration parameters of the initial system, including curvature radii of the PM, SM, and TM, and the distances between them based on the method above. In order to correct the residual aberration, we set the radii, distances, and conic coefficients as variables in optical design software for initial optimization. The optical layout of the obtained initial structure is shown in Fig. 4, and the parameters are listed in Table 2.

4. OPTICAL SYSTEM OPTIMIZATION

After obtaining the initial structure, we move the aperture stop from the TM to the front of the focal plane and make it offset to avoid the central obscuration. The FOV is not biased to avoid extra off-axis aberration. In this paper, we adopt a progressive optimization strategy to obtain an ideal final system, and the FOV is expanded gradually during the optimization process.

Before optimization, operands, and constraints provided by optical design software ZEMAX should be setting to constrain the geometric and optical features of the system. To prevent the window glass from blocking the light reflected from the SM to the TM, a virtual surface with the same axial position as the window glass is set between the SM and the TM. Then we set an operand combination of RAGY and OPGT to make the height of the light passing through the bottom of the virtual surface greater than that passing through the top of the window glass. The same operand combination is also used to prevent the three mirrors from blocking light. In order to ensure that the aperture stop and the focal plane are coaxial, we added the operand RAID to control the incident angle of the chief ray at the central FOV at the focal plane to zero. The coordinates of the chief rays at the marginal FOV striking the focal plane were constrained by the operand REAR to control the distortion.

In the process of expanding the FOV, we set the decenter and tilt of mirrors as variables to eliminate the ray obscuration and increase the aberration correction ability of the system. Considering the necessity of reducing the alignment difficulty, we restrict the tilt amount of each mirror to less than 5°. For the purpose of keeping the optical system symmetrical about the meridian plane, the decenter and tilt of mirrors are only carried out in the YZ plane.

In the first step of optimization, the FOV is set as 2° × 1°, and the window glass was inserted into the system at this stage. A large amount of residual aberration was generated on the marginal FOV, and the average root-mean-square (RMS) wavefront error is about 0.52λ (λ = 4.2 μm) because of the aperture stop offset. The surfaces of the three mirrors were replaced with even aspheric surfaces, and the 4th and 6th aspheric terms of all surfaces were set as variables. After a round of optimization, the average RMS wavefront error is reduced to 0.06λ. In the second step of optimization, the FOV is expanded to 4° × 3°. Due to the FOV expansion, the average RMS wavefront error increased to 0.43λ. Through the analysis, we find that there is a large amount of astigmatism in the system, and the PM and TM contribute the most to the correction of astigmatism. Therefore, the 8th and 10th aspheric terms of the PM and TM are set as variables to offer a higher degree of freedom to balance the aberration. After optimization, the average RMS wavefront error reaches 0.07λ. In the third step, the FOV is expanded from 4° × 3° to the maximum FOV, i.e., 5.3° × 4.4°. In this step, we found that the residual aberration of the marginal FOV is difficult to correct due to the limited system optimization degrees of freedom, especially when the aperture stop is placed between the TM and focal plane which makes the system asymmetric and thus contributes less to correct lateral aberration. Therefore, increasing optimization degrees of freedom is a necessary and effective measure to achieve an ideal image quality. Freeform surfaces belong to the field of non-rotationally symmetric surfaces which have stronger aberration correction ability compared with conventional optical surfaces owing to more design and optimization degrees of freedom [33]. Among the kinds of freeform surfaces, the Zernike polynomial surface and XY polynomial (extended polynomials in x, y) surface are the representative ones. Compared with the Zernike polynomial surface, the XY polynomial surface is easier to process because it coincides with the numerical control optical manufacturing expression form and is fit to model certain expressions [34]. Therefore, we adopt the XY polynomial surface to correct the residual aberrations of the marginal FOV in our system. The equation of XY polynomial is

$$Z = \frac{cr^2}{1 + \sqrt{1 - (1+k)\,c^2 r^2}} + \sum_{i=2}^{66} C_i x^m y^n, \tag{13}$$

where Z is the surface sag, c is the surface curvature, k is the conic constant, and C_i is the term coefficient. In most optical design software, the highest order of the XY polynomial is usually 10, i.e., $m + n \le 10$.

Among the three mirrors in this system, the TM plays the most important role in correcting aberration, especially the

Table 3. Polynomial Parameters of the Freeform TM

Term	Coefficient	Term	Coefficient
X^0Y^1	0.7173	X^0Y^3	0.0128
X^2Y^0	−0.0715	X^4Y^0	−3.7791*e*-003
X^0Y^2	−0.0401	X^2Y^2	1.2693e-003
X^2Y^1	0.0144	X^0Y^4	1.1467e-003

astigmatism through our analysis; thus, we converted the TM surface to an XY polynomial surface. In order to simplify the optimization process and ensure that the TM and the whole system are symmetrical about the tangential plane, the coefficients of odd order terms of x are fit to 0; thus, only even order terms of x are retained. After the final optimization, we obtained an ideal design result with high image quality. The average RMS wavefront of the final system is 0.04λ. The highest-order aspherical terms of both the PM and SM are all 10th terms. The XY polynomial coefficients of the TM are listed in Table 3. The total axial length of this optical layout is about 435 mm, as shown in Fig. 5.

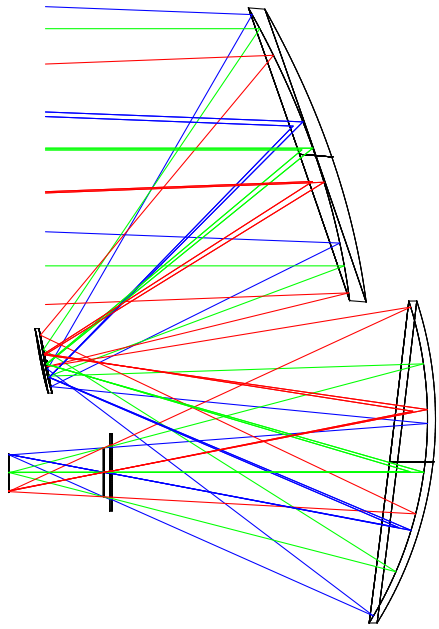

Fig. 5. Optical layout of the optimized system, which has a reasonable structure and ideal image quality.

5. IMAGE PERFORMANCE AND TOLERANCE ANALYSIS

A. Image Performance

In our system, the diameter of the aperture stop is 50 mm, and the distance from it to the focal plane is 100 mm. Thus, the aperture stop can match the cold stop of the detectors we choose, and the stray radiation can be suppressed effectively. The MTF is an important index to measure the image quality. As is shown

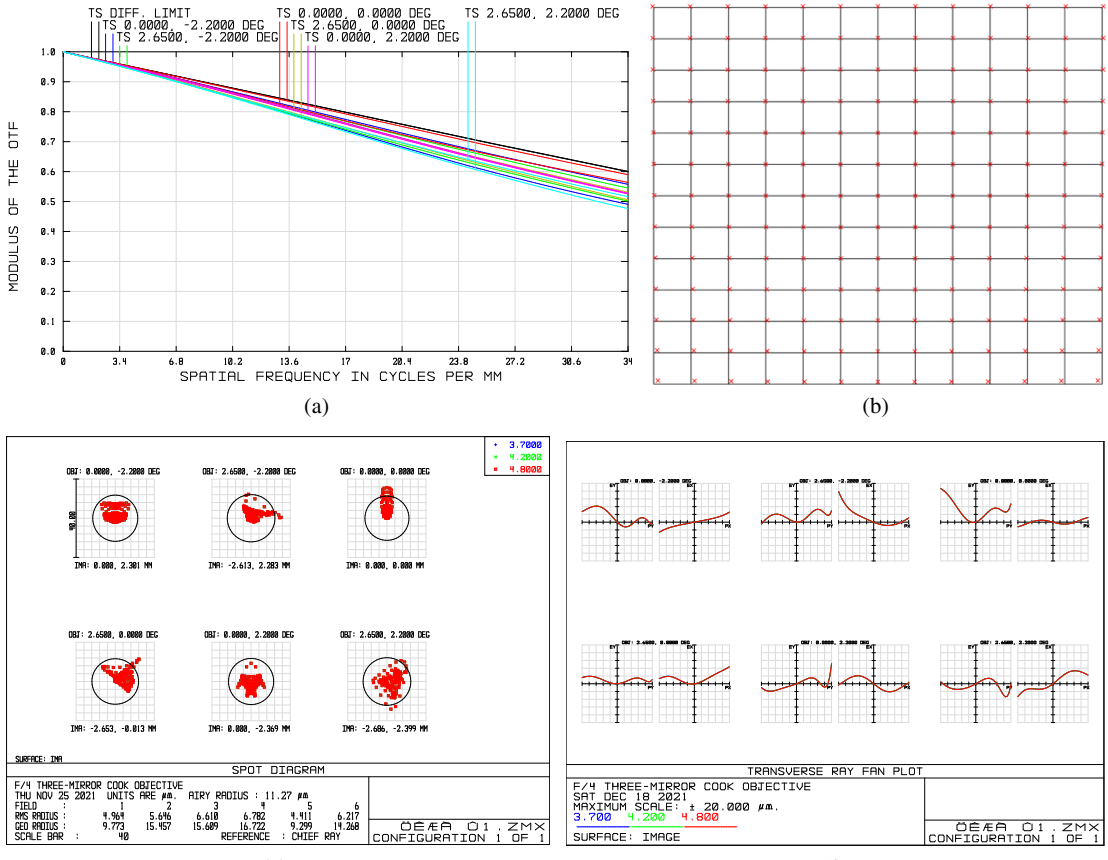

Fig. 6. Image quality of the optical system: (a) MTF, (b) grid distortion, (c) spot diagram, and (d) ray fans.

Table 4. Tolerance Allocation of the Optical System

	Shape Error RMS (λ)	Radius (mm)	Conic	Decenter (mm)	Tilt (″)	Distance (mm)
PM	1/50	±0.005	±0.0005	±0.01	±30	±0.05
SM	1/50	±0.01	±0.001	±0.01	±30	±0.05
TM	1/50	±0.01	±0.001	±0.01	±20	±0.05

in Fig. 6(a), the MTF over the whole FOV exceeds 0.45 at 34 lp/mm, approaching the diffraction limitation, which is better than the design requirement. During the optimization process, the distortion value of the system is set as a merit function, and the grid distortion is shown in Fig. 6(b), where the black grid and red crosses represent the position of paraxial image and real image points, respectively. The magnitude of the maximum distortion is 1.86% at the marginal FOV, and it needs to be corrected by the image processing algorithm. The spot diagram of the system is shown in Fig. 6(c). It can be seen that the radii over the full FOV are close to that of the Airy spot, and the RMS diameters are less than one single pixel size (15 μm), meaning a high resolution of the system. The ray fans display ray aberrations as a function of the pupil coordinate, from which we can intuitively observe various aberrations of the optical system. Figure 6(d) shows the ray fans of our system, in which the maximum corresponding coordinate scale is 20 μm, meaning a good aberration correction result.

B. Tolerance Analysis

The tolerance analysis is used to evaluate the feasibility of practical application of the optical system, which is determined by the capacity of fabrication and alignment. We can systematically analyze the influence of slight error such as surface irregularity, mirror decenter, and tilt on system performance. In the process of the tolerance analysis, we take the average diffraction MTF at 34 lp/mm as an evaluation criterion and the distance from the aperture stop to the focal plane as the compensation. The tolerance values are shown in Table 4. The results of the tolerance analysis show that under the given tolerance allocation, the average diffraction MTF at 34 lp/mm is better than 0.28 with a probability of 90%, which means that the system has excellent instrumentation feasibility.

6. CONCLUSION

The research in the fields of infrared detection with high precision and a wide scale, and the design of the corresponding optical system, are of great value. In order to realize the detection goal, a cooled off-axis three-mirror MWIR optical system with a wide FOV, long focal length, and large relative aperture has been successfully designed in this paper. The initial coaxial three-mirror configuration is solved analytically based on the third-order Seidel aberration theory, and the progressive optimization method is described in detail. The system adopts aspheric surfaces with high-order terms and an XY polynomial surface to increase the optimizing degrees of freedom and improve the aberration correction ability of the system. The XY polynomial surface in this system also plays a key role in achieving a compact layout. The spectral range is 3.7–4.8 μm, with a 5.3° × 4.4° FOV, 500 mm focal length, and 2F-number. The MTF of this system exceeds 0.45 when the spatial frequency is 34 lp/mm, and the distortion is constrained within a reasonable range. The diameter and the position of the aperture stop enable it to match with the cold stop of the infrared detector. The characteristics of our system enable it to realize high-precision and wide-scale infrared remote sensing. In addition, the design methods presented in this paper can provide technical reference for the development of an infrared optical system with similar specifications. We have also carried out the tolerance analysis to demonstrate the feasibility and reliability of practical application of the optical system. If the other two mirrors also adopt a freeform surface, the system can theoretically achieve better performance such as a wider FOV and better image quality. We will delve into the relevant research in our future work.

Funding. National Natural Science Foundation of China (62175236).

Disclosures. The authors declare no conflicts of interest.

Data availability. Data underlying the results presented in this paper are not publicly available at this time but may be obtained from the authors upon reasonable request.

REFERENCES

1. L. Zhao, Z. Luan, Y. Xiong, and L. He, "Athermalization design of wide field medium wave infrared optical system," Adv. Mater. Res. **981**, 295–298 (2014).
2. X. Q. Ai, B. Liu, X. Zhang, and H. G. Jia, "Thermal difference analysis and athermalization design of infrared optical system," Proc. SPIE **7849**, 78491P (2010).
3. H. E. John, V. Niumsawatt, W. M. Rozen, and I. S. Whitaker, "Clinical applications of dynamic infrared thermography in plastic surgery: a systematic review," Gland Surg. **5**, 122–132 (2016).
4. Y. L. Ma, W. Z. Liu, and W. S. Wang, "Optical system design of a new type infrared dual-band seeker," Proc. SPIE **7544**, 75443X (2010).
5. Y. Zhang, J. Y. Shang, X. Yue, and W. S. Wang, "Design of cooled athermalized infrared telephoto lens," Proc. SPIE **8557**, 855716 (2012).
6. H. Z. Dang, L. B. Wang, Y. N. Wu, K. X. Yang, S. S. Li, and W. B. Shen, "Development of a 2.0 W at 60 K single-stage coaxial pulse tube cryocooler for long wave infrared focal plane array applications," Proc. SPIE **7660**, 76602S (2010).
7. A. Manissadjian, P. Tribolet, P. Chorier, and P. Costa, "SOFRADIR infrared detector products: the past and the future," Proc. SPIE **4130**, 480–495 (2000).
8. H. H. Martijn and J. Y. Andersson, "On-chip analog to digital conversion for cooled infrared detector arrays," Proc. SPIE **4028**, 183–191 (2000).
9. E. Mohammadi, M. Ghaffari, and N. Behdad, "Wide dynamic range, angle-sensing, long-wave infrared detector using nano-antenna arrays," Sci. Rep. **10**, 2488 (2020).
10. Z. H. Shi, L. Yu, D. S. Cao, Q. W. Wu, X. Y. Yu, and G. Y. Lin, "Airborne ultraviolet imaging system for oil slick surveillance: oil-seawater contrast, imaging concept, signal-to-noise ratio, optical design, and optomechanical model," Appl. Opt. **54**, 7648–7655 (2015).
11. X. H. Wang, X. Zhong, R. F. Zhu, and F. Gan, "Nadir and omnidirectional limb imaging spectrometer based on acousto-optic tunable filter," Opt. Commun. **437**, 81–89 (2019).
12. Q. S. Xue, Z. T. Tian, B. Yang, J. S. Liang, C. Li, F. P. Wang, and Q. Li, "Underwater hyperspectral imaging system using a prism-grating-prism structure," Appl. Opt. **60**, 894–900 (2021).
13. K. Dong, L. Zhang, J. Wang, H. Wang, Q. Sun, and Z. Lu, "Design of the infrared dual-band athermalized optical system based on HDE," Proc. SPIE **7383**, 73831B (2009).
14. W. Wang, X. Zhong, J. Liu, and X. H. Wang, "Apochromatic lens design in the short-wave infrared band using the Buchdahl dispersion mode," Appl. Opt. **58**, 892–903 (2019).

15. X. J. Li, C. B. Zou, and J. T. Yang, "Design of image-side telecentric off-axis three-mirror anastigmatic systems based on the coaxial parent mirrors," Optik **241**, 166855 (2021).
16. Q. Y. Meng, H. Y. Wang, K. J. Wang, Y. Wang, Z. H. Ji, and D. Wang, "Off-axis three-mirror freeform telescope with a large linear field of view based on an integration mirror," Appl. Opt. **55**, 8962–8970 (2016).
17. J. Zhu, W. Hou, X. D. Zhang, and G. Jin, "Design of a low F-number freeform off-axis three-mirror system with rectangular field-of-view," J. Opt. **17**, 015605 (2015).
18. H. R. Ji, Z. B. Zhu, H. Tan, Y. F. Shan, W. Tan, and D. L. Ma, "Design of a high-throughput telescope based on scanning an off-axis three-mirror anastigmat system," Appl. Opt. **60**, 2817–2823 (2021).
19. Q. Y. Meng, H. Y. Wang, W. J. Liang, Z. Q. Yan, and B. W. Wang, "Design of off-axis three-mirror systems with ultrawide field of view based on an expansion process of surface freeform and field of view," Appl. Opt. **58**, 609–615 (2019).
20. Q. Y. Meng, H. Y. Wang, W. Wang, and Z. Q. Yan, "Desensitization design method of unobscured three-mirror anastigmatic optical systems with an adjustment-optimization-evaluation process," Appl. Opt. **57**, 1472–1481 (2018).
21. L. G. Cook, "Method and apparatus for receiving optical signals," U.S. patent 4834517 (30 May 1989).
22. L. G. Cook, "Compact four-mirror anastigmat telescope," U.S. patent US20030179443 (25 September 2003).
23. Q. H. Yu, X. S. Mao, F. S. Chen, and S. L. Sun, "Design method for triple conjugate optical system with good stray light control performance," J. Infrared, Millimeter, Terahertz. Waves **38**, 8–14 (2019).
24. X. Jiang, X. Jia, and S. Cong, "Application of freeform surfaces in cooled off-axis three-mirror optical system," Infrared Laser Eng. **47**, 0918004 (2018).
25. C. Cao, S. Liao, Z. Liao, Y. Bai, B. Chen, and Z. Fan, "Design of cooled freeform-surface off-axis reflective optical system," Acta Opt. Sin. **39**, 0808001 (2019).
26. W. J. Smith, *Modern Optical Engineering*, 4th ed. (2007).
27. Y. Q. Xie, C. Y. Liu, S. Liu, and X. H. Fan, "Optical design of imaging spectrometer based on linear variable filter for nighttime light remote sensing," Sensors **21**, 4313 (2021).
28. C. Han, *MTF Analysis and Radiation Calibration of Space Camera* (Science, 2005).
29. J. M. Rodgers, "Unobscured mirror designs," Proc. SPIE **4832**, 33–60 (2002).
30. L. G. Cook, "Three mirror anastigmatic optical system," U.S. patent 4265510 (5 May 1981).
31. W. B. Wetherell and D. A. Womble, "All-reflective three element objective," U.S. patent 4240707 (23 December 1980).
32. L. G. Cook, "Reflective optical triplet having a real entrance pupil," U.S. patent 4733955 (29 March 1988).
33. T. Yang, D. W. Cheng, and Y. T. Wang, "Direct generation of starting points for freeform off-axis three-mirror imaging system design using neural network based deep-learning," Opt. Express **27**, 17228–17238 (2019).
34. Q. Y. Meng, W. Wang, H. C. Ma, and J. H. Dong, "Easy-aligned off-axis three-mirror system with wide field of view using freeform surface based on integration of primary and tertiary mirror," Appl. Opt. **53**, 3028–3034 (2014).

221.8.12.133 {ts '2023-02-28 21:09:05'}